IEEE Access
Multidisciplinary | Rapid Review | Open Access Journal

Received April 30, 2019, accepted May 16, 2019, date of publication May 22, 2019, date of current version June 6, 2019.

Digital Object Identifier 10.1109/ACCESS.2019.2918343

Detection for Incipient Damages of Wind Turbine Rolling Bearing Based on VMD-AMCKD Method

JUN ZHANG[1], JIANQUN ZHANG[1], MIN ZHONG[1], JIANHUA ZHONG[1], JINDE ZHENG[2], AND LIGANG YAO[1]

[1]School of Mechanical Engineering and Automation, Fuzhou University, Fuzhou 350116, China
[2]School of Mechanical Engineering, Anhui University of Technology, Maanshan 243032, China

Corresponding author: Jun Zhang (zhang_jun@fzu.edu.cn)

This work was sponsored in part by the National Natural Science Foundation of China under Grant 51875105, Grant 51775114, and Grant 51505002.

ABSTRACT Incipient damages of wind turbine rolling bearing are very difficult to be detected because of the interference of multi-frequency components and strong ambient noise. To solve this problem, this paper proposes a new detected method named VMD-AMCKD, combining complementary advantages of variational mode decomposition (VMD) and adaptive maximum correlated kurtosis deconvolution (AMCKD). A novel index is proposed to screen out the most sensitive mode containing fault information after VMD decomposition. The mode also can determine a suspectable range for the fault frequency, based on which the optimized range of devolution period T in MCKD can be pre-determined. The Grasshopper optimization algorithm (GOA) is adapted to adaptively select the key parameters in MCKD. The proposed method can successfully diagnose the simulated signal mixed with strong white Gaussian noise. Its robustness is further proven by the diagnosis for three different types of experimental signal from CWRU bearing data center. Finally, the VMD-AMCKD is applied to detect incipient damages of rolling bearings in a laboratory wind turbine.

INDEX TERMS Incipient damage detection, rolling bearing, wind turbine, variational mode decomposition, adaptive maximum correlated kurtosis deconvolution, grasshopper optimization algorithm.

I. INTRODUCTION

Due to the features of abundance, cleanness and renewability, wind power resource has received increasing attentions from the academic and industrial fields in recent years [1], [2]. To harvest the wind energy, plenty of wind turbines have been built and applied every year. However, wind turbines are vulnerable to maintain normal operations because of their extremely severe working conditions. Among all the factors leading to functional failure of wind turbines, the most frequent and influential one is bearing failure [3]. Incipient damages of rolling bearing may result in significant bearing fault, causing damages to other components. Therefore, it is of great importance to detect incipient damages of rolling bearing before they arouse catastrophic results. However, incipient damages of rolling bearings are very difficult to be detected [4]. The reason may lie in that the fault features of rolling bearing arousing from incipient damages are usually very weak, which are very likely submerged either by multi-frequency information or by strong background noise.

The associate editor coordinating the review of this manuscript and approving it for publication was Francesco Tedesco.

In general, the collected vibration signal of mechanical systems is a superposition of vibration information of each component and background noise [5]. Thus, signal decomposition is often used to filter out noise and get a sensitive mode containing fault information for fault identification [6]. For this purpose, many signal processing methods, including classic wavelet decomposition [7], empirical mode decomposition (EMD) [8] and local mean decomposition (LMD) [9] have been developed in recent decades. These methods have achieved commendable results in the field of fault identification, however, they still have the following problems. For the classic wavelet decomposition, it is difficult to choose suitable wavelet base functions and decomposition layers regarding to different actual signals. The recursive mode decomposition methods such as EMD and LMD have no strict mathematical derivation and still suffer from the end effect.

To eliminate the modal aliasing and the end effect, Dragomiretskiy and Zossot [10] proposed variational mode decomposition (VMD) in 2014. Since its proposition, the analysis methods based on VMD have been developed rapidly and applied widely. For instance, Satish *et al.* [11] proved that VMD outperforms EMD in diagnosing fault

signal of rolling bearings. Zhang *et al.* [12] applied VMD to identify the damage type in multistage centrifugal pump. For the studies of [11] and [12], the parameters of K and α in VMD were determined with the authors' prior knowledge. However, the fact is that an inappropriate choice for the parameters of K and α in VMD will lead to incorrect decomposition results. So as to implement adaptive determination of VMD parameters, Yan *et al.* [13] used the genetic algorithm (GA) to optimize α and K. In order to avoid mode mixing in VMD, Li *et al.* [14] determined the mode number K with the peak searching method.

Though VMD can extract fault features through signal decomposition, Reference [15] proved that it fails to fully extract all fault information under strong background noise. To suppress the heavy noise, maximum correlated kurtosis deconvolution (MCKD) was proposed and has been widely applied in fault detection [16]–[19]. For example, Zhao and Li [17] used MCKD to successfully suppress the noise when diagnosed the weak fault of wind turbine bearings. By adopting MCKD with improved spectral kurtosis, Wan *et al.* [18] and Jia *et al.* [19] achieved satisfactory diagnosis effects of early bearing faults. However, in these investigations, the period of deconvolution T and the length of filter L in MCKD were determined either by authors' experience or by prior knowledge. To solve this problem, Tang and Wang [20] adopted the particle swarm optimization (PSO) to select L and T when conducted MCKD. Pitifully, they did not explain how to determine an optimized range for the parameter of T. Because the parameter of T is closely related to the bandwidth that may contain the fault characteristic frequency, pre-process the signal to make sure it contains fault features before carrying out MCKD is necessary. To improve the diagnosis efficiency, one may need an intelligent optimization algorithm to shorten the searching time for the MCKD parameters. Among all the intelligent optimization algorithms, the grasshopper optimization algorithm (GOA) has been proved being superior over other optimization algorithms such as PSO, GA and etc. [21].

In view of the above studies, it can be found that adopting VMD under strong background noise can hardly achieve desirable diagnostic results while using MCKD without signal pre-processing may miss suspectable fault frequency. Since the vibration signals of wind turbine rolling bearings often subjects to heavy noise and multi-frequency interference, it naturally comes to the author that we can combine the two algorithms of VMD and MCKD to utilize their complementary advantages for incipient damage detection. To be specific, we can use VMD for signal pro-processing, i.e., to obtain the most sensitive mode of original signal containing fault information. Meanwhile, through VMD we can determine a suspectable range for the fault frequency, based on which the optimized range of devolution period T can be pre-determined. Then we adopt the intelligent optimization algorithm GOA to fulfil an adaptive selection of the period of deconvolution T and the length of filter L in MCKD. We named the optimized MCKD algorithm as AMCKD. Finally, the most sensitive component of the original signal is further used to carry out AMCKD to obtain the weak fault features. This is the basic idea of VMD-AMCKD method.

Bearing with the above idea, the subsequent sections of this article are arrayed as follows. In Section II, the theoretical foundations of VMD-AMCKD are briefly introduced. The detailed steps of VMD-AMCKD are described in Section III followed by its application to a widely used simulation signal in Section IV. In section V, three cases of CWRU bearing data center are used to demonstrate the robustness of VMD-AMCKD method. In Section VI, two kinds of incipient damage of rolling bearings in a laboratory wind turbine are detected by the proposed method. End of this paper, some conclusions are summarized in Section VII.

II. THEORETICAL FOUNDATIONS OF VMD-AMCKD

The theoretical foundations of three algorithms of VMD, MCKD and GOA involved in the proposed method are briefly introduced for better understanding of VMD-AMCKD method in this section.

A. BRIEF INTRODUCTION OF VMD

VMD aims to decompose a real-valued input signal x into a series of discrete modes u_k with certain sparsity properties [10]. All frequency components of each mode are concentrated near a center frequency ω_k. The bandwidth of each mode is reckoned by the squared L^2 norm of the gradient. The sum of all u_k equivalents to x as a constraint. Therefore, the construction and solution of variational mode decomposition is considered as the constrained variational problem described by the following equation.

$$\begin{cases} \min\limits_{\{u_k\},\{\omega_k\}} \left\{ \sum\limits_{k=1}^{K} \left\| \partial_t \left[\left(\delta(t) + \dfrac{\mathrm{j}}{\pi t} \right) * u_k(t) \right] e^{-j\omega_k t} \right\|_2^2 \right\} \\ s.t. \sum\limits_{k=1}^{K} u_k = x \end{cases} \tag{1}$$

where $\{u_k\} := \{u_1, \ldots, u_K\}$, $\{\omega_k\} := \{\omega_1, \ldots, \omega_K\}$; K is the decomposition mode number; $\delta(t)$ represents the Diarc distribution; t indicates the time; j is an imaginary unit; "$*$" represents a convolution operation; $\partial t(\cdot)$ is a function seeking partial derivative of t.

To solve the problem of (1), the Lagrangian multiplier λ and the quadratic penalty term α are used to make the problem unconstrained. Herein, λ can enhance the constrained stringency while α can effectively guarantee reconstructed accuracy. The augmented Lagrangian is described as follow.

$$\begin{aligned} &L(\{u_k\}, \{\omega_k\}, \lambda) \\ &= \alpha \sum_{k=1}^{K} \left\| \partial_t \left[\left(\delta(t) + \frac{j}{\pi t} \right) * u_k(t) \right] e^{-j\omega_k t} \right\|_2^2 \\ &\quad + \left\| x(t) - \sum_{k}^{K} u_k(t) \right\|_2^2 + \left\langle \lambda(t), x(t) - \sum_{k=1}^{K} u_k(t) \right\rangle \end{aligned} \tag{2}$$

Thus, the solution of (1) is transformed into finding the saddle point of (2). Firstly, K, the frequency domain expression of mode $\hat{u}_k^1$, the corresponding center frequency ω_k^1 and a Lagrangian multiplier $\hat{\lambda}^1$ are initialized. Therefore, u_k, ω_k can update according to (3) and (4), respectively.

$$\hat{u}_k^{n+1}(\omega) = \frac{\hat{x}(\omega) - \sum_{g>k} \hat{u}_g^{n+1}(\omega) - \sum_{g>k} \hat{u}_g^{n+1}(\omega) + \frac{\hat{\lambda}^n(\omega)}{2}}{1 + 2\alpha\left(\omega - \omega_k^n\right)^2} \tag{3}$$

$$\omega_k^{n+1} = \frac{\int_0^\infty \omega \left|\hat{u}_k^{n+1}(\omega)\right|^2 d\omega}{\int_0^\infty \left|\hat{u}_k^{n+1}(\omega)\right|^2 d\omega} \tag{4}$$

where $g \in [1, K]$, n is the number of iterations.

With modes and the center frequencies acquired by (3) and (4), the Lagrangian multipliers is renewed through the following equation.

$$\hat{\lambda}^{n+1}(\omega) \leftarrow \hat{\lambda}^n(\omega) + \Gamma\left(\hat{x}(\omega) - \sum_k \hat{u}_k^{n+1}(\omega)\right) \tag{5}$$

where Γ is an updated factor and represents the noise-tolerance.

The above iteration of (3), (4) and (5) is continued until convergence, namely

$$\sum_{k=1}^{K} \left\| u_k^{n+1} - u_k^n \right\|_2^2 / \left\| u_k^n \right\|_2^2 < \varepsilon \tag{6}$$

where ε is a positive value for precision.

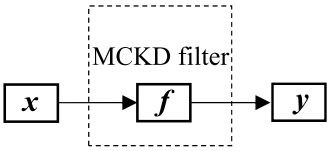

FIGURE 1. Principle of MCKD algorithm.

B. BRIEF INTRODUCTION OF MCKD

MCKD is a method to extract weak impact components from low SNR (signal-to-noise ratio) signal by raising the kurtosis of signals [16]. When neglecting the influence of noise, one can define the discrete signal x_i as the response excited by a fault impulse signal y_i. maximum correlated kurtosis deconvolution is used to find a series of FIR filter f_l to maximize the correlated kurtosis of y_i recovered from the responsive signal x_i as described in (7) and in Fig.1.

$$\boldsymbol{y} = \boldsymbol{f} * \boldsymbol{x} = \sum_{l=1}^{L} f_l x_{i-l+1} \tag{7}$$

where $\boldsymbol{y}$, $\boldsymbol{x}$ are the vectors of y_i, x_i; $\boldsymbol{f} = [f_1\ f_2 \ldots f_L]^{\mathrm{T}}$; $l = 1, 2, \ldots, L$ with L being the filter length.

The definition of correlated kurtosis can be expressed as.

$$CK_M(T) = \frac{\sum_{i=1}^{N}\left(\prod_{m=0}^{M} y_{i-mT}\right)^2}{\left(\sum_{i=1}^{N} y_i^2\right)^{M+1}} \tag{8}$$

where T is the period of deconvolution; N is the length of collected signal and M is the number of conversion. Increasing M will increase the number of pulses. But for a large M, the iterative method will result in a loss of numerical precision [17]. In the present study, M is set as 7.

The optimized function of maximum correlated kurtosis deconvolution can be defined as.

$$\max_f CK_M(T) = \max_f \frac{\sum_{i=1}^{N}\left(\prod_{m=0}^{M} y_{i-mT}\right)^2}{\left(\sum_{i=1}^{N} y_i^2\right)^{M+1}} \tag{9}$$

Equation (9) is used to get the most suitable filter which can maximize the correlated kurtosis. The calculated equation is expressed as,

$$\frac{d}{df_l} CK_M(T) = 0 \quad (l = 1, 2, \cdots, L) \tag{10}$$

Further, the final solution of $\boldsymbol{f}$ is expressed as

$$\boldsymbol{f} = \frac{\|\boldsymbol{y}\|^2}{2\|\boldsymbol{\beta}\|^2}\left(\boldsymbol{X}_0 \boldsymbol{X}_0^T\right)^{-1} \sum_{m=0}^{M} \boldsymbol{X}_{mT} \boldsymbol{\psi}_m \tag{11}$$

where

$$\boldsymbol{\beta} = \begin{bmatrix} y_1 y_{1-T} \cdots y_{1-MT} \\ y_2 y_{2-T} \cdots y_{2-MT} \\ \vdots \\ y_N y_{N-T} \cdots y_{N-mT} \end{bmatrix}_{N\times 1};$$

$$\boldsymbol{X}_r = \begin{bmatrix} x_{1-r} & x_{2-r} & x_{3-r} & \cdots & x_{N-r} \\ 0 & x_{1-r} & x_{2-r} & \cdots & x_{N-1-r} \\ 0 & 0 & x_{1-r} & \cdots & x_{N-2-r} \\ \vdots & \vdots & \vdots & \ddots & \vdots \\ 0 & 0 & 0 & \cdots & x_{N-L-r+1} \end{bmatrix}_{L\times N},$$

$$r = [0\ T\ 2T\ \cdots\ mT];$$

$$\boldsymbol{\psi}_m = \begin{bmatrix} y_{1-mT}^{-1}\left(y_1^2 y_{1-T}^2 \cdots y_{1-MT}^2\right) \\ y_{2-mT}^{-1}\left(y_2^2 y_{2-T}^2 \cdots y_{1-MT}^2\right) \\ \vdots \\ y_{N-mT}^{-1}\left(y_N^2 y_{N-T}^2 \cdots y_{N-MT}^2\right) \end{bmatrix}_{N\times 1}.$$

C. BRIEF INTRODUCTION OF GOA

GOA is one of nature-inspired algorithm that simulates the process of grasshoppers prey in nature [21]. Their behavior can be expressed as a mathematic model as the follow.

$$P_i = S_i + G_i + W_i \tag{12}$$

where P_i represents the position of the i-th grasshopper; S_i and G_i represents the social interaction and the gravity force on the i-th grasshopper, respectively; W_i represents the wind advection.

Usually, a modified equation as expressed in (12) is adopted to simplify the above equation when applying the GOA algorithm. Herein, the gravity (G_i) is omitted; the social interaction(S_i) is optimized; the wind direction (W_i) is supposed to be always towards the optimal target. The position of the i-th grasshopper in the d-th dimension can be calculated by following equation.

$$P_i^d = c\left(\sum_{j=1,j\neq i}^{N'} c\frac{ub_d - lb_d}{2} s\left(\left|p_j^d - p_i^d\right|\right)\frac{p_j - p_i}{d_{ij}}\right) + \hat{T}_d \tag{13}$$

where c is a decreasing coefficient; $j \in [1, N']$, N' is the size of grasshopper swarms; ub_d and lb_d are the upper and the lower bounds in the d-th dimension; $s(\bar{r}) = f_0 e^{-\bar{r}/l_0} - e^{-\bar{r}}$, generally, $f_0 = 1.5$ and $l_0 = 0.5$ are chosen [21]; $d_{ij} = |p_i\text{-}p_j|$ is the distance between the i-th and the j-th grasshopper; $\hat{T}_d$ is the optimization target. As can be seen from (13), the next position of the grasshopper is determined by its current position, optimal target, and the positions of other grasshoppers.

To achieve a better optimized effect, the decreasing coefficient c adopts a linearly-varying dynamic value:

$$c = c_{\max} - h\frac{c_{\max} - c_{\min}}{H} \tag{14}$$

where h is the number of current iteration; H is the maximum number of total iterations; $c_{\max}$ and $c_{\min}$ are the maximum and minimum decreasing coefficients. The parameter c ensures that the GOA algorithm can't converge to the target too quick, thereby avoiding local optima and accelerating the convergence speed in the last few iterations.

When using the GOA to optimize the MCKD parameters, a fitness function needs to be determined. In this paper, the fitness function adopts the value of crest factor of envelope spectrum (Ec) which was proposed in [22]. Assuming that envelope spectrum amplitude sequence of the signal is $X(z)$ ($z = 1, 2, \ldots, Z$), Ec can be expressed as

$$Ec = \frac{\max(X(z))}{\sqrt{\sum_z X(z)^2/Z}} \tag{15}$$

where $X(z)$ is the amplitude of envelope spectrum within the frequency range of $[f_r', \gamma f_i']$. Herein, f_r' is larger than the maximum rotational frequency of the shaft in the drive system. f_i' is the maximum rolling bearing fault characteristic frequency of the system; and $\gamma \in [4, 8]$.

A high value of Ec means a strong periodic impact, thus representing a more distinct fault feature. Since the objective of GOA optimization is to find the minimum value, the value of '$-Ec$' is served as the objective function in VMD-AMCKD.

```
Initialize the swarm P_i (i=1, 2, …, N)
Initialize c_max, c_min, and maximum number of iterations
Calculate the fitness of each search agent
P = the best search agent
while (l < Max number of iterations)
   Update c
   for each search agent
      Normalize the distances between grasshoppers in [1, 4]
      Update the position of the current search agent
      Bring the current search agent back if it goes outside boundaries
   end for
   Update P, if there is a better solution
   h=h+1
end while
Return P
```

FIGURE 2. Pseudo code of the GOA algorithm.

Fig.2 is a pseudo code of the GOA algorithm that can express the main steps of optimization process.

III. PRINCIPLE AND DESCRIPTION OF VMD-AMCKD METHOD

The flowchart of VMD-AMCKD method is illustrated in Fig.3. As can be seen from the above figure, there are several key points for this newly proposed method: (1) How to determine K. (2) How to select the most sensitive mode. (3) How to determine the optimal range of parameter T. The detailed steps of VMD-AMCKD as listed below:

Step 1: Determine the key parameters of α and K in VMD and then apply VMD to analyze the input signal. Herein, $\alpha = 2000$ is set, which is its default value of [10]. The decomposition mode number K is determined by center frequency observation to avoid mode mixing. The detailed determination process of K is addressed as follows. 1) Initialize $K = 2$.2) Update K with $K = K + 1$.3) Carry out VMD and compare the maximum value of center frequency $\omega_{\max}^K$ and $\omega_{\max}^{K-1}$ produced in the K-th iteration and (K-1)-th iteration. The calculation of the central frequency is determined by (4), that is, the center frequency is calculated by power spectrum. 4) Stop the iteration when $\omega_{\max}^K$-$\omega_{\max}^{K-1} \leq 0.01 f_s$. 5) Selected $K = K - 1$ as the decomposition mode number.

Step 2: Select the most sensitive mode and determine the optimized range of deconvolution period T. When selecting the most sensitive mode, the distribution density of impact impulses and the correlation between the component and the whole should be considered [6]. An index CEc is proposed to combine the correlated coefficient C and crest factor of envelope spectrum Ec as defined in (20), which can be expressed as follows.

$$CEc = |C| \cdot Ec \tag{16}$$

$$C = \frac{\mathrm{E}[(u_k - \bar{u}_k)(x - \bar{x})]}{\mathrm{E}\left[(u_k - \bar{u}_k)^2\right]\mathrm{E}\left[(x - \bar{x})^2\right]} \tag{17}$$

where $|C|$ is an absolute value of the correlated coefficient between a component signal u_k and the original signal x;

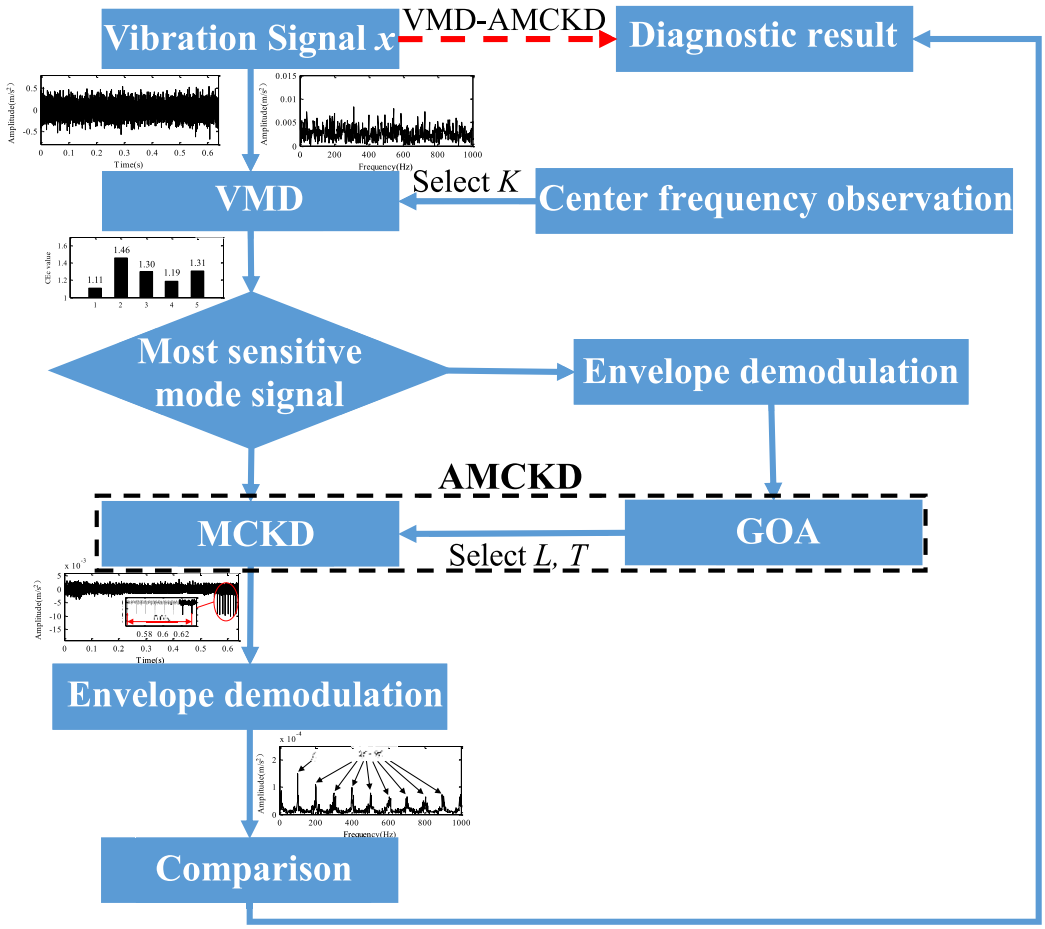

FIGURE 3. Flowchart of VMD-AMCKD.

E(·) represents the mathematical expectation; $\bar{u}_k$ and $\bar{x}$ represent the average value of the signal sequence.

On the basis of above definitions, the most sensitive mode can be selected through the maximum value of *CEc* index according to the VMD decomposing results of fault signals. The selected most sensitive mode is then analyzed by envelope demodulation. From the envelope spectrum, the frequency f_{d} corresponding to the largest amplitude is selected as the central value of suspectable fault frequency interval. It should be noted that f_{d} cannot be the frequency of the known motor input speed. With the determined central value f_{d}, the suspectable fault frequency interval can be set. Note that this interval of suspectable fault frequency should be appropriate: a small interval may not contain the fault frequency while a large interval will increase the computation cost. Based on our tremendous practices, we recommend the interval as $f_a = [0.8f_{\mathrm{d}}, 1.2f_{\mathrm{d}}]$. After determining the suspectable fault frequency interval, the optimized range of the deconvolution period T can be calculated as

$$T = f_s/f_a \tag{18}$$

where f_s is the sampling frequency.

Step 3: Optimize the key parameters of L and T in MCKD algorithm with GOA and use MCKD to pick up the characteristic information from the most sensitive mode signal. Set the parameters of $N' = 30$ and $H = 15$. Set the optimized range of parameter L as [100, 1000].

Step 4: Extract incipient fault features of damaged bearing through the Hilbert envelope demodulation. The frequency corresponding to the spectral line with obvious peak in the envelope spectrum is often selected as the suspectable fault frequency.

Step 5: Compare the extracted suspectable fault frequency with the theoretical fault characteristic frequency and identify the damage type and location.

IV. APPLICATION TO A SIMULATED SIGNAL

In this section, a pulsed signal proposed by [20], [23], [24] is used to inspect the validity of the VMD-AMCKD method in detecting incipient damage of rolling bearing inner race. The simulated signal can be formulated as

$$\begin{cases} x(t) = \sum_{\kappa} A_\kappa h(t - \kappa T_1 - \tau_\kappa) + n(t) \\ A_\kappa = A_0 \sin(2\pi f_r t) + C_A \\ h(t) = \exp(-C_0 t) \sin(2\pi f_n t) \end{cases} \tag{19}$$

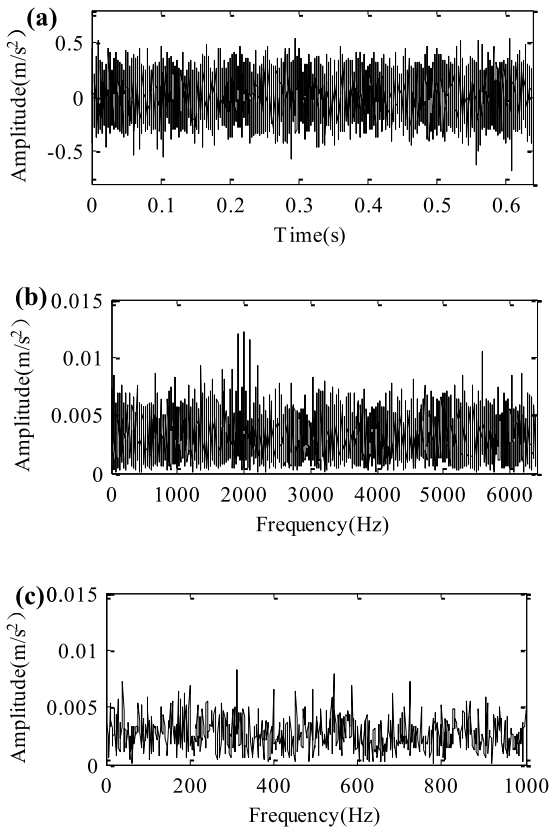

FIGURE 4. Waveform and spectrum of the simulated signal: (a) time waveform; (b) frequency spectrum and (c) envelope spectrum.

where A_κ is amplitude modulation with a period of $1/f_r$ and f_r is the rotation frequency of the axis; $h(t)$ is the oscillating impulse with an average inter-arrival time T_1; τ_κ is the small fluctuation of κ-th impact around T_1; n(t) represents a white Gaussian noise with SNR of -17dB. In the present study, $f_r = 20$ Hz; $T_1 = 0.01$ s and it means that fault characteristic frequency f_i is 100 Hz; $A_0 = 0.5$; C_A is an arbitrary constant; $C_0 = 800$; $f_n = 2000$ Hz. 8192 points are analyzed for this case while the sampling frequency f_s is 12800 Hz.

The time waveform, the spectrum and the envelope spectrum of the simulated signal as illustrated in Fig. 4.

From Fig. 4(a), there are no significant periodic impulses in the time waveform. All periodic features of original impulse signal are completely submerged by the white Gaussian noise. Consequently, it can hardly identify fault information from Fig. 4(b), Fig. 4(c). This manifests that traditional time–domain analysis and the traditional spectrum analysis fail to detect the incipient damage of rolling bearing under strong background noise. The following will demonstrate how to use the proposed VMD-AMCKD method to detect the impact pulse in the simulated signal.

Firstly, determining K according to Step 1 as described in Section 3. As shown in Table 1, The center frequency ω_k of each mode according to different updating K is calculated.

From Table 1, one can find that. $\omega^6_{\max}$-$\omega^5_{\max} = 5835.8 - 5805.4 = 30.4 \leq 0.01\, f_s = 128$. Therefore, the decomposition mode number is determined as $K = 5$.

After determining K, the original signal is decomposed through variational mode decomposition with $\alpha = 2000$ and $K = 5$. The results after VMD analysis are illustrated in Fig. 5.

There are five modes is clearly observed from Fig. 5. Meanwhile, the bandwidth of each individual decomposition mode doesn't overlap. This proves that the selection of $K = 5$ is proper in that it doesn't arouse mode mixing.

Secondly, calculating the value of *CEc* for each decomposition mode according to (16) and selecting the most sensitive mode according the calculation results. The calculation results are illustrated in Fig. 6.

As can be observed from the figure that the second mode u_2 claims the largest value of *CEc*. Therefore, u_2 is selected as the most sensitive mode to perform envelope demodulation. The result is illustrated in Fig. 7.

As can be seen in Fig. 7, the characteristic frequency corresponding to the large amplitude is $f_d = 120.3$ Hz. Therefore, the suspectable fault frequency interval of f_a is set as [96, 144]. Hence, the optimized range of period deconvolution T can be defined as [89, 133] according to (18) as described by Step 2 in Section 3. In addition, it is worthy to point out that it is difficult to extract the fault features through envelope demodulation of the most sensitive mode obtained from VMD. Besides, there exists three prominent spectral lines whose amplitude is very approximate. This implies that using VMD independently under strong background noise fails to achieve desirable fault diagnosis results.

Thirdly, optimizing the parameters of L and T in MCKD with GOA. To be more specific, the fitness function curve

TABLE 1. ω_k of each mode according to different updating K.

K	ω_k/Hz					
	u_1	u_2	u_3	u_4	u_5	u_6
2	1540.4	3604.4				
3	587.1	2024.1	4742.9			
4	567.1	1952.1	3575.3	5367.4		
5	554.1	1903.5	3336.5	4674.4	5805.4	
6	446.9	1498.3	2490	3573.8	4726.7	5835.8

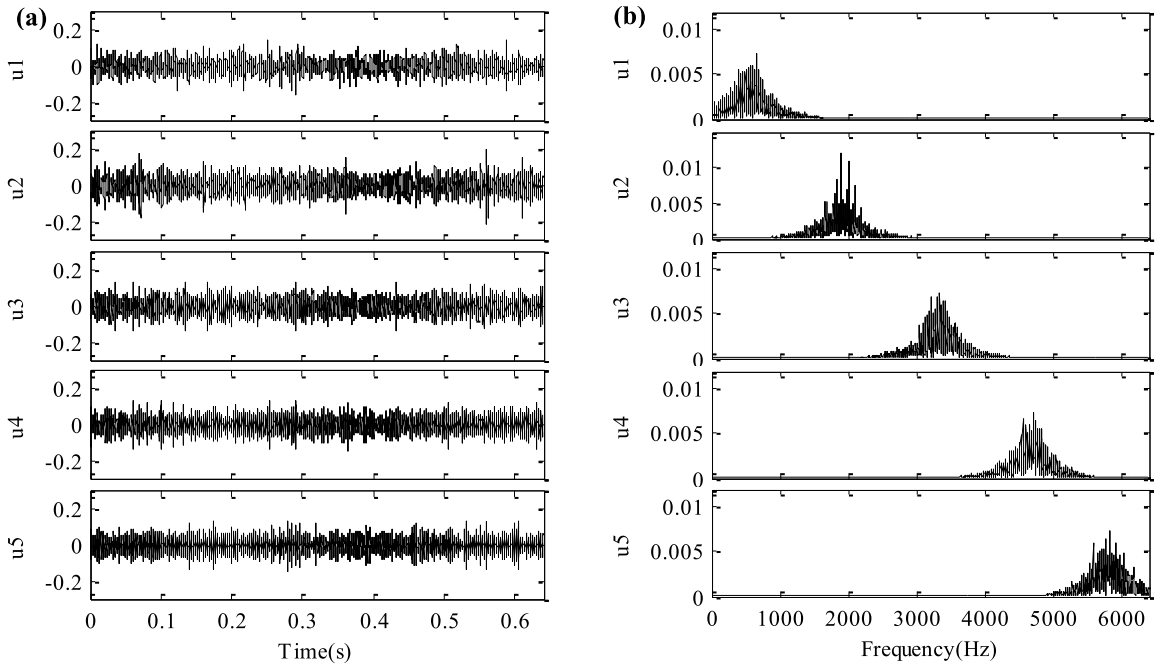

FIGURE 5. Decomposition results of the simulated signal through VMD: (a) time waveforms of component signals; (b) spectrum of component signals.

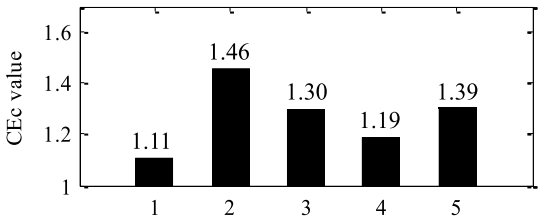

FIGURE 6. *CEc* values of the decomposition modes.

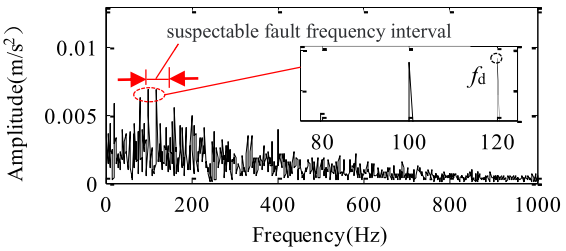

FIGURE 7. The Hilbert envelope spectrum of the most sensitive mode.

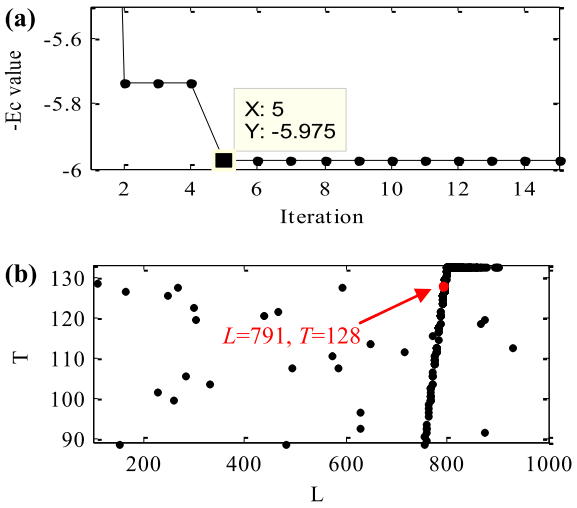

FIGURE 8. GOA results: (a) fitness function curve; (b) historical locations of grasshoppers.

and the historical locations of grasshoppers are illustrated in Fig. 8.

From Fig. 8(a) that GOA converges at the fifth generation can be observed. From Fig. 8(b), it can be found that the optimal parameters are $L = 791$ and $T = 128$.

Fourthly, based on the optimized parameters of L and T, an AMCKD analysis for the most sensitive mode is carried out to obtain its time waveform and envelope spectrum. The results after VMD-AMCKD analysis are shown in Fig. 9.

In the time waveform from Fig. 9(a), the pulsed information can obviously be observed. The duration of seven impacts marked in the figure is 0.07s, which is consistent with the single shocked period $T_1 = 0.01$s. In other words, the pulsed frequency f_i is 100 Hz as aforementioned in (19). From Fig. 9(b), the fault frequency f_i as well as its harmonics ($2f_i$, $3f_i$, …, $9f_i$) can be seen clearly. It indicates that the validity of the VMD-AMCKD method.

To illustrate the necessity of optimizing parameters of L and T through GOA, we set $T = 120$, which varies within 10% from the original parameter of $T = 128$. Fig.10 (a) shows the envelope spectrum obtained by the non-optimized parameters [791, 120] of MCKD for the most

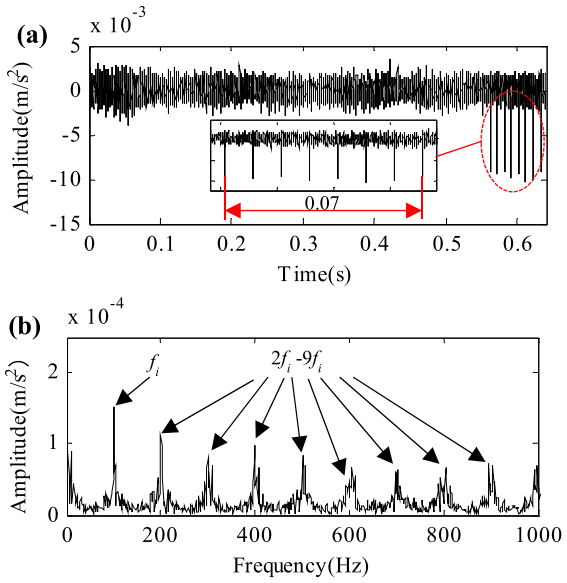

FIGURE 9. The results after VMD-AMCKD analysis: (a) time waveform; (b) envelope spectrum.

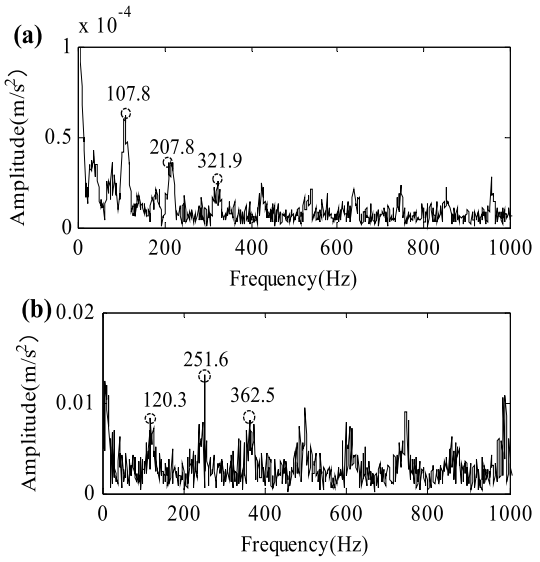

FIGURE 10. Envelope spectra: (a) with non-optimized T; (b) the original signal after AMCKD analysis.

sensitive mode. Similarly, to illustrate the necessity of preprocessing the original signal with VMD, Fig. 10(b) illustrates envelop spectrum of the original signal by applying AMCKD directly with the same optimized range of $T = [89, 133]$.

Although some prominent spectral lines can be observed from Fig. 10(a), none of them corresponds to the fault frequency. It proves that the key parameters must be optimized by GOA before carrying out an AMCKD. Similarly, the protruding frequencies appeared in Fig. 10(b) don't correspond to the fault frequency f_i and the harmonics as well. It implies that using AMCKD alone for the original signal analysis cannot achieve correct diagnosis results. The results shown in Fig. 10 also reversely prove the necessity of combining VMD and AMCKD algorithms simultaneously. In summary, the proposed method of VMD-AMCKD can suppress background noise and can enhance transient continuous impact in weak fault signals, thus, is capable of detecting incipient damages of rolling bearings.

V. ROBUSTNESS VERIFICATION OF VMD-AMCKD

In this section, three sets of bearing fault data originated from the Case Western Reserve University(CWRU) bearing data center [25] are used to demonstrate the robustness of VMD-AMCKD. The fault data sets were collected from an experimental bearing test rig with an incipient localized damage on the inner race, the rolling element and the outer race, respectively. More details of these data sets can refer to [26] and [27], in which a detailed benchmark study was conducted in [26]. More recently, these data sets were further used to proof the effectiveness of Autogram method of selecting the optimal band for bearing fault diagnosis proposed by Ali Moshrefzadeh in [27].

A. CASE 1: INCIPIENT DAMAGE ON THE INNER RACE

Record 275 DE with an incipient damage on the inner race of rolling bearing is examined in this case. The damage is difficult to be detected because of the impulsive noise [27]. Damaged diameter of the electric spark machining is 0.3356 mm. On the basis of input speed of the system and the damaged bearing parameters, the fault frequency f_i of this signal is calculated as 148.2 Hz. The sampling frequency f_s in this examination is 12 kHz and 8192 points are analyzed for this case.

The time waveform of the raw signal, the envelope spectrum of the most sensitive mode after VMD decomposition, the time waveform and its envelope spectrum after VMD-AMCKD analysis are shown in Fig. 11(a)-(d), respectively.

It can be found that the total time of 18 impact cycles in the figure is 0.61s from Fig. 11(a). Obviously, single impact cycle that is easy to be calculated is 0.034s, corresponding the shaft speed 29.33 Hz. By applying VMD-AMCKD according to the aforementioned steps, the following results are obtained. Herein, VMD decomposition number K is determined as 2 by the method of center frequency observation. The values of CEc of the two decomposition components are calculated as 2.973 and 5.489, respectively. Hence, u_2 is determined as the most sensitive mode. From Fig. 11(b), the most prominent spectra line locates at 29.33 Hz can be found, which equals to the rotating frequency of the motor f_r. Therefore, f_d is determined as 146.5 Hz by the spectra line with the second largest amplitude. The suspectable fault frequency interval is obtained as [117.2, 175.8] Hz, leading to an optimal range of $T = [68, 103]$ according (18). With the determined range of T, the key parameters are optimized by GOA, yielding the results of $L = 342$ and $T = 84$.

As illustrated in Fig. 11(d), the fault frequency f_i, and $2f_i$, $3f_i$, $4f_i$ can be clearly seen from the envelope spectrum, the validity of this method is proved. The proposed method

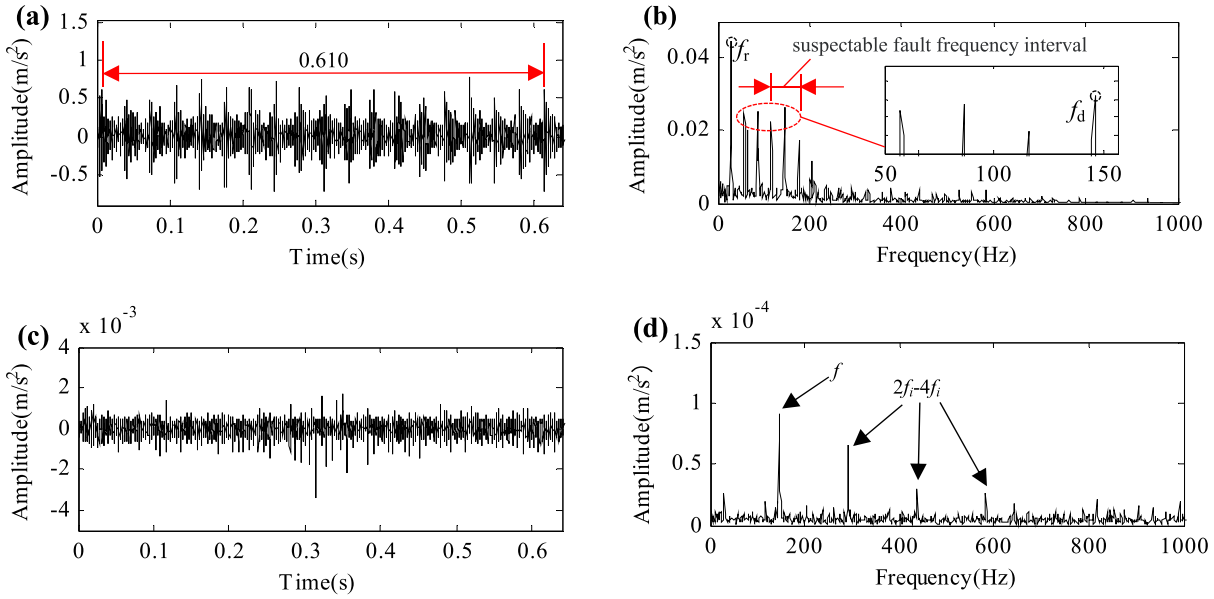

FIGURE 11. Analysis of Case 1 with impulsive noise: (a) time waveform of the raw signal; (b) envelope spectrum of the most sensitive mode; (c) time waveform after VMD-AMCKD analysis; (d) envelope spectrum after VMD-AMCKD analysis.

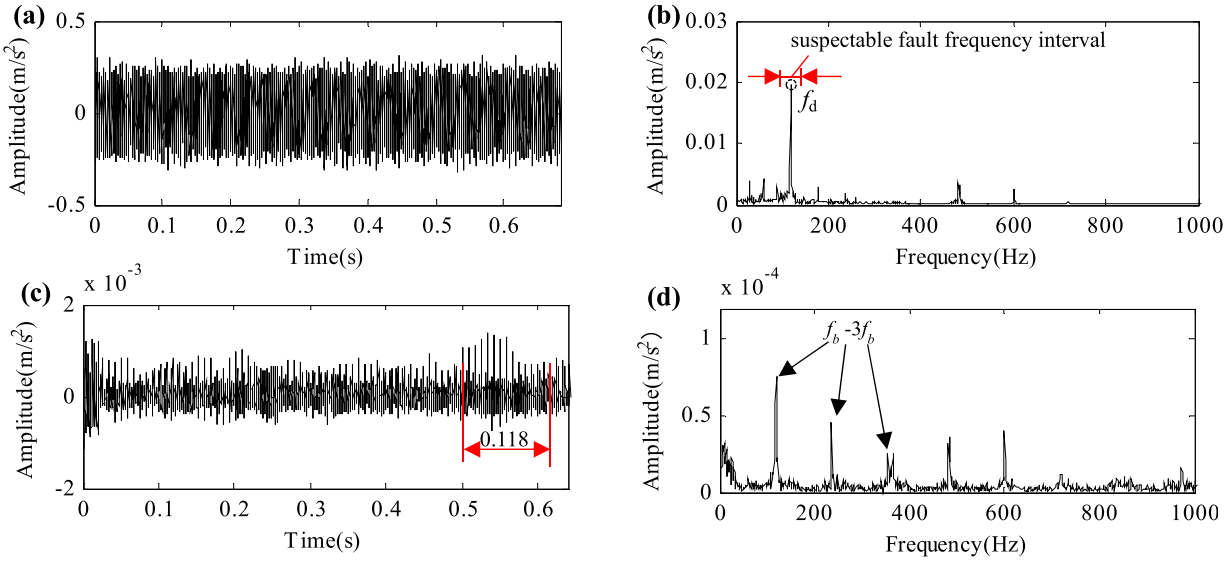

FIGURE 12. Analysis of Case 2 with several non-periodic impulses: (a) time waveform of the original signal; (b) envelope spectrum of the most sensitive mode; (c) time waveform after VMD-AMCKD analysis; (d) envelope spectrum of (c).

in [27] can detect the fault signal as well. However, there are many interference frequencies around the fault frequency. For the fault signal detection of record 275 DE, the VMD-AMCKD method has better diagnostic results than the method proposed in [27].

The above analysis proves that VMD-AMCKD method is capable of diagnosing signals containing impulsive noise with high accuracy.

B. CASE 2: INCIPIENT DAMAGE ON THE ROLLING ELEMENT

In this case, record 291 BA with an incipient damage on the rolling element of the rolling bearing is examined. The damage is difficult to be detected due to several non-periodic impulses [27]. Damaged diameter of the electric spark machining is 0.5334 mm. By calculation, the rolling element fault characteristic frequency f_b of this case is 117.8 Hz. The sampling frequency f_s of this examination is 12 kHz and 8192 points are analyzed for this case.

Its time waveform is illustrated in Fig. 12 (a), from which the impact time interval related to the rolling element fault frequency can't be observed distinctly. Following steps of VMD-AMCKD method, one may obtain the envelope spectrum of the most sensitive mode after VMD analysis, the time waveform and its envelope spectrum after VMD-AMCKD analysis as shown in Fig. 12(b)-(d), respectively.

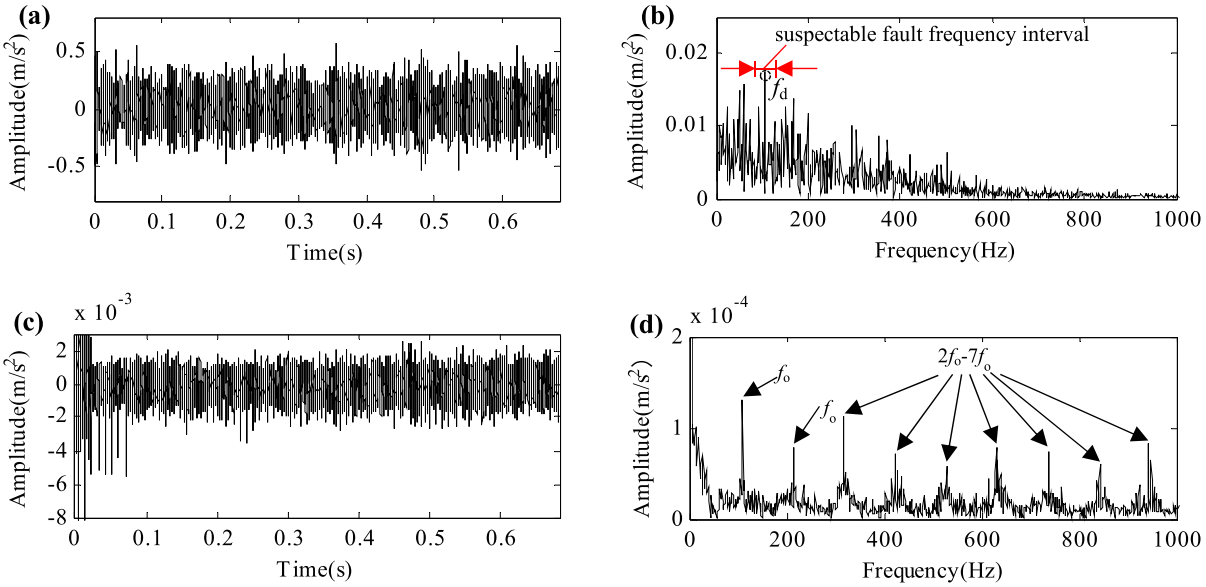

FIGURE 13. Analysis of Case 3 with low signal to noise ratio: (a) time waveform of the original signal; (b) envelope spectrum of the most sensitive mode; (c) time waveform after VMD-AMCKD analysis; (d) envelope spectrum of (c).

Herein, the VMD decomposition number is determined as $K = 2$; the values of *CEc* of the two modes are calculated as 2.167 and 16.114, respectively. From envelope spectrum of the u_2 as shown in Fig. 12(b), f_d is determined as 118.7 Hz. And an interval of [94.96, 142.44] is used to calculate the optimized range of the deconvolution period $T = [84, 127]$. The optimal parameters obtained from the GOA algorithm are $L = 264$ and $T = 99$.

From the time waveform of the filtered signal, one can find that the total time of 14 impact cycles in the figure is 0.118s. Obviously, single impact cycle that is easy to be calculated is 0.00843s, corresponding the frequency speed 118.7 Hz. From Fig. 12(d), the rolling element fault characteristic frequency f_b and its multiple frequencies can be seen expressly.

The analysis results of this case indicate the capability of VMD-AMCKD method suppressing non-periodic impulses.

C. CASE 3: INCIPIENT DAMAGE ON THE OUTER RACE

In this case, record 203 DE with an incipient damage on the rolling bearing outer race is examined. The damage is difficult to be detected because of low SNR [27]. Damaged diameter of electric spark machining is 0.3356 mm. By calculation, the outer race fault frequency f_o for this case is 104.6 Hz. The sampling frequency f_s is 48 kHz and 32768 points are analyzed for this case.

Its time waveform is illustrated in Fig. 13(a), from which the impact time interval associated with the fault frequency can't be observed directly. Following steps of VMD-AMCKD method, one may obtain the envelope spectrum of the most sensitive mode after VMD analysis, the time waveform and its envelope spectrum after VMD-AMCKD analysis as illustrated in Fig. 13(b)-(d), respectively.

Herein, VMD decomposition number K is set as 4. The *CEc* values of u_i $(i = 1, 2, 3, 4)$ are 1.0153, 4.2348, 3.5870 and 0.9546, respectively. Therefore, u_2 is selected as the most sensitive mode. From the envelope spectrum of u_2, f_d can be determined as 105.5 Hz, leading to an suspectable fault frequency interval of [84.4, 126.6] Hz and an optimized range of the $T = [379, 569]$. In the AMCKD algorithm, the optimal parameters are $L = 1000$, $T = 456$. From the Fig. 13(d), f_o and its multiple frequencies could be clearly seen.

Above analysis results verify the capability of VMD-AMCKD in dealing with low SNR signals.

D. DISCUSSIONS

To further highlight the effectiveness and robustness of the proposed method, one may compare the results of the above three examples with the results obtained from the benchmark study. Table 2 shows the results of analysis of VMD-AMCKD method with those from appendix tables in [26].

Through the comparative analysis of the above table, the robustness of VMD-AMCKD is well proved.

From all the cases in this section, it can be concluded that VMD-AMCKD method is effective and robust in detecting incipient damages of rolling bearing, including the inner race damage, rolling element damage and outer race damage as well.

VI. DETECTION FOR INCIPIENT DAMAGES OF WIND TURBINE ROLLING BEARINGS

In this section, two sets of faulty bearing signals are collected from a SQ wind turbine simulator (WTS) in our laboratory are analyzed with VMD-AMCKD method. The analysis results are further compared with that obtained from MED-SK. Herein, the effectiveness of VMD-AMCKD method in detecting incipient damages of wind turbine rolling bearings is verified.

TABLE 2. Comparison of VMD-AMCKD with benchmark study.

Data Record	Reasons for Difficulty of Diagnosis	VMD-AMCKD	Envelope analysis (Method 1 in [26])	Cepstrum prewhitening (Method 2 in [26])	Benchmark method (Method 3 in [26])
275 DE	impulsive noise	√	—	—	×
291 BA	non-periodic impulses	√	√	×	×
203 DE	low SNR	√	—	—	—

where "√" represents data clearly diagnosable; "—" represents data probably diagnosable; "×" represents data not diagnosable.

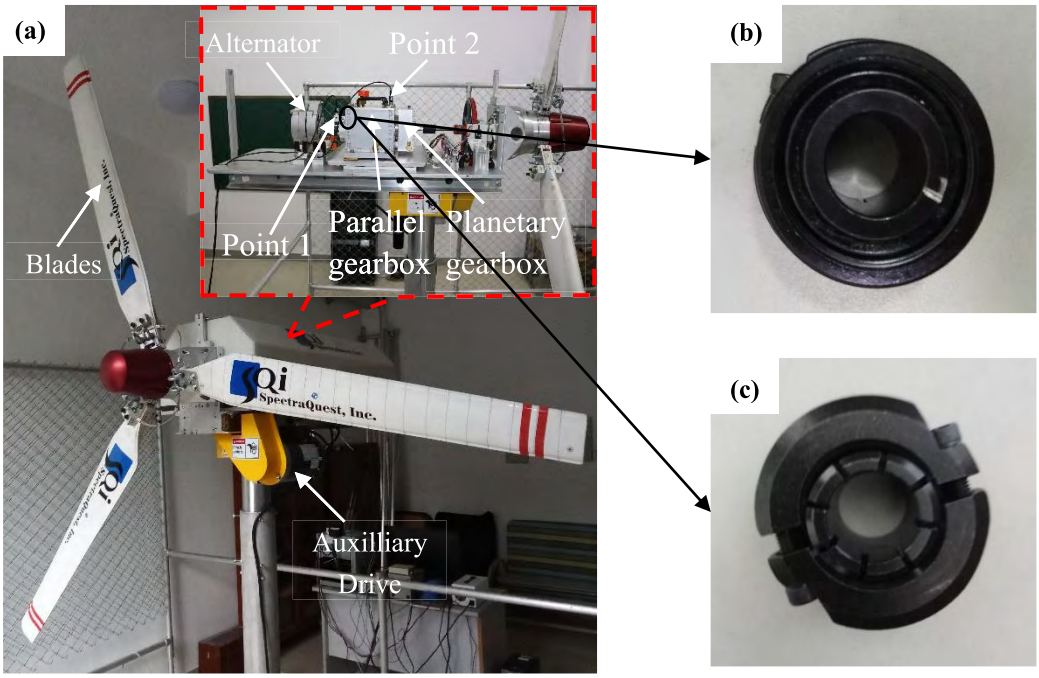

FIGURE 14. (a) WTS test-rig; (b) bearing with inner race damage; (c) bearing with rolling ball damage.

A. DATA ACQUISITION

A laboratory WTS is applied to generate the experimental signals of wind turbine rolling bearing with incipient damages. As illustrated in Fig. 14(a), the WTS mainly consists of an auxiliary motor, three blades, a planetary gearbox, a parallel shaft gearbox, and a generator. In the wind turbine driven system, the transmission ratio of the planetary gearbox is 4.571; the transmission ratio of the first stage and the second stage of the parallel shaft gearbox is 2.683 and 1.210, respectively. The damaged bearing is located at the end of the driven shaft in the first stage transmission of the parallel shaft gearbox. The type of damaged rolling bearing is ER-12K. Damages on inner race and rolling element of rolling bearings are set as illustrated in Fig. 14.

The structural parameters of the damaged bearings are illustrated in Table 3, according to which the shaft rotating frequency, the theoretical fault frequencies are calculated are illustrated in Table 4.

TABLE 3. Structural parameters of the damaged bearing.

Parameters	Value
Pitch diameter(mm)	33.4772
Contact angle (°)	0
Ball diameter(mm)	7.9375
Number of balls	8

In the present study, the sampling frequency f_s for fault signal with inner race damage and rolling ball damage is set as 12800 Hz and 6400 Hz, respectively. The sampling points of the two cases are set as 8192. The input speed provided by the motor is 0.991 Hz. A Gaussian noise with SNR of

TABLE 4. Fault characteristic frequencies of the damaged bearing.

Frequency column	Value(Hz)
Rotational frequency f_r	12.15
Inner race fault frequency f_i	$4.95\times f_r$=60.16
Outer race fault frequency f_o	$3.048\times f_r$=37.04
Ball fault frequency f_b	$1.992\times f_r$=24.21
Cage fault frequency f_c	$0.378\times f_r$=4.59

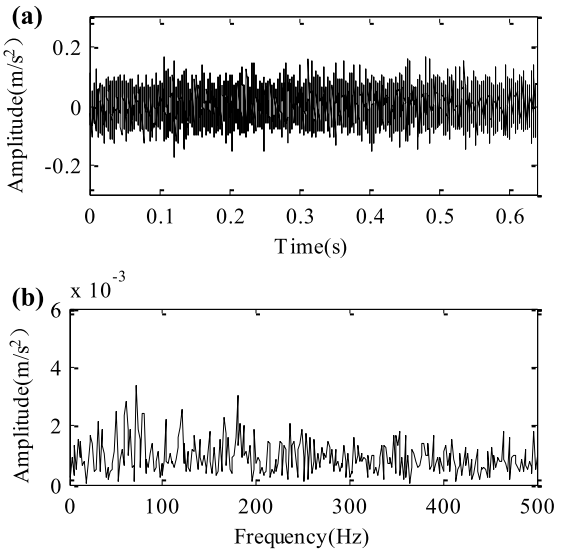

FIGURE 15. Case 1: (a) time waveform of signal with inner race damage; (b) envelope spectrum of (a).

−4dB is added to the raw signal collected at the measuring point 1 to compound an experimental signal. In such a way, the compounded experimental signal will be closer to the real-world signal when the wind turbine works under actual conditions.

B. CASE 1: INCIPIENT DAMAGE ON THE INNER RACE

Fig. 15(a) and 15(b) show the time waveform and envelope spectrum of the fault signal of rolling bearing with inner race damage, respectively. In the time waveform, no impulse components can be observed. The spectra lines are very messy in the Fig. 15(b). It's difficult to find damage information from the raw signal.

VMD-AMCKD is used to processing the fault signal for this case. Firstly, according to the steps of selecting K, the parameter of K is set as 5. Secondly, calculating the value of *CEc* with the range of *Ec* setting as [20, 500]. Fig. 16 shows the *CEc* value of each mode.

As can be seen from Fig. 16, u_1 is selected as the most sensitive mode to perform envelope demodulation. The result is shown in Fig. 17.

A protruding frequency of $f_d = 60.94$ Hz can be observed in Fig. 17 and a suspectable fault frequency interval [48.75, 73.13] is selected to yield an optimized range of period deconvolution T as [175, 263]. After then, the MCKD

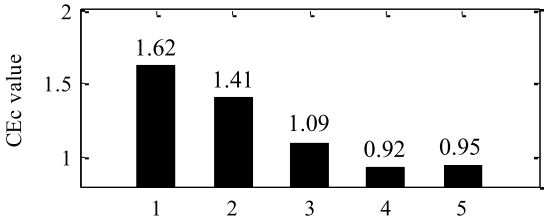

FIGURE 16. Case 1: *CEc* values of the decomposition modes.

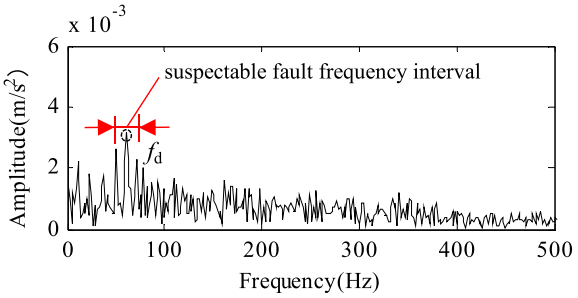

FIGURE 17. Case 1: The envelope spectrum of u_1.

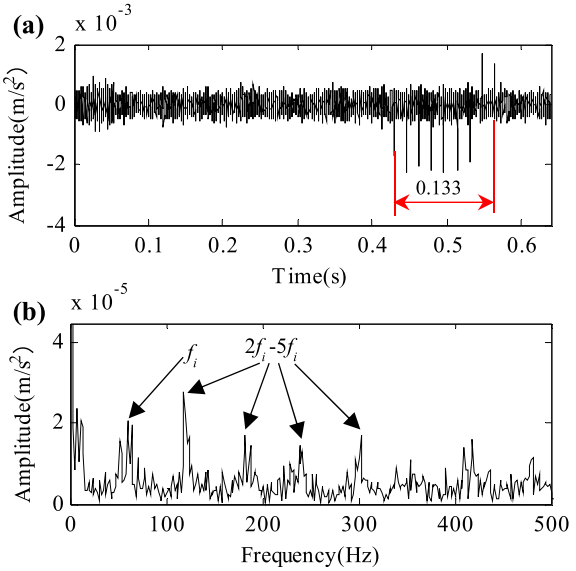

FIGURE 18. Case1: The results of VMD-AMCKD analysis: (a) time waveform; (b) envelope spectrum.

parameter combination $[L, T]$ can be optimized by the GOA. The optimal parameters are set as $L = 678$ and $T = 214$.

Based on the optimized parameters of L and T, an AMCKD analysis for the most sensitive mode is carried out. The results of VMD-AMCKD analysis are shown in Fig. 18.

From Fig. 18(a), the fault information can be observed obviously. The time duration of eight shocked cycles adds up to 0.133s, which means that the fault frequency extracted by VMD-AMCKD is 60.15 Hz. In the processed envelope spectrum, the fault frequency f_i as well as the harmonics (2-$5f_i$) can be distinctly visible. It indicates that the fault

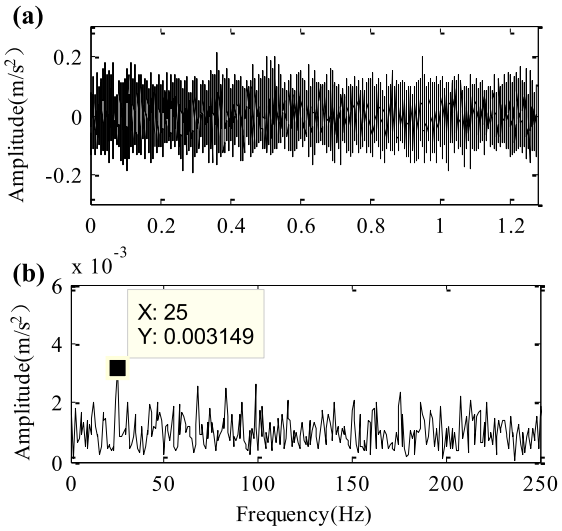

FIGURE 19. Case2: (a) time waveform; (b) envelope spectrum of (a).

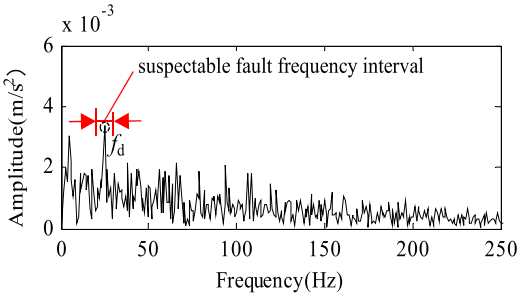

FIGURE 20. Case2: Envelope spectrum of the most sensitive mode.

features coming from the inner race damage are accurately extracted.

C. CASE 2: INCIPIENT DAMAGE ON THE ROLLING ELEMENT

The time waveform and its envelope spectrum of the fault signal of wind turbine rolling bearing with rolling element damage are illustrated in Fig. 19(a) and (b), respectively.

In the time waveform, some impulse components are capable of being observed. In the envelope spectrum, the spectra lines are very messy. It's difficult to observe useful fault features from these bearing signals.

In order to obtain fault information from the fault signal, VMD-AMCKD method is applied. Firstly, according to the steps of selecting K, the decomposition mode number K is set as 5.

After VMD decomposition, u_3 can be selected as for further analysis due to the maximum CEc of u_3. Note that the calculation range of the Ec index is set as [20, 300]. The envelope spectrum of u_3 is shown in Fig. 20.

As can be seen from Fig. 20, the suspectable fault characteristic frequency f_d is 25 Hz. Therefore, an interval of [20, 30] is used to calculate the range of AMCKD optimized parameter T. After optimization, the optimal parameters are

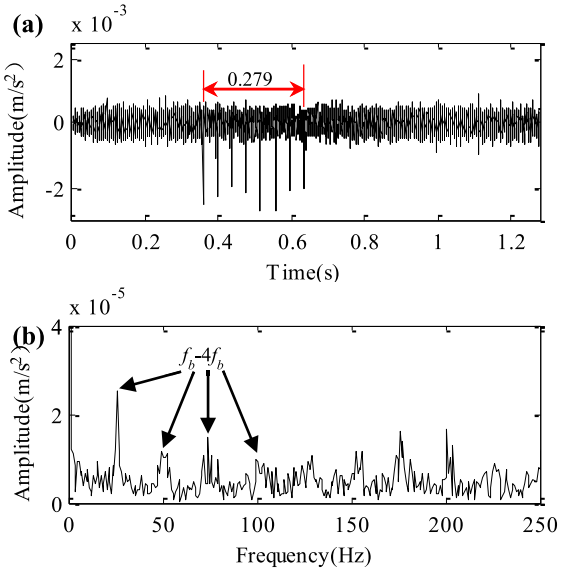

FIGURE 21. Case 2: The results of VMD-AMCKD analysis: (a) time waveform; (b) envelope spectrum.

set as $L = 656$ and $T = 254$. Based on the optimal parameters, the AMCKD analysis for the most sensitive mode is carried out. The results after VMD-AMCKD analysis are illustrated in Fig. 21.

In the time waveform as illustrated in Fig. 21(a), some shock impulses can be observed obviously. The time duration of seven shocked cycles adds up to 0.279s, which means that the fault characteristic frequency extracted by VMD-AMCKD is 25.09 Hz. It differs from the theoretical fault frequency 24.21 Hz, which is most likely due to the sliding effect of bearing [28]. In the envelope spectrum as illustrated in Fig. 24(b), the fault frequency f_b as well as its harmonics is clearly illustrated. This manifests that the fault features coming from the rolling element damage are accurately extracted.

D. COMPARISON WITH MED-SK

It has been proven by [28] and [29] that minimum entropy deconvolution (MED) combined with spectral kurtosis(SK) can extract incipient fault features of damaged bearings. In this subsection, the above experimental signals are analyzed by MED-SK method and above results are compared with those obtained from VMD-AMCKD method proposed in this paper. Reference [17] shows that in the MCKD algorithm, when $T = 0$, $M = 1$, the MCKD algorithm degenerates into the MED algorithm. In such a way, the MED algorithm is mainly affected by the filter length L.

1) MED-SK BASED DETECTION FOR INNER RACE DAMAGE OF ROLLING BEARING

For comparison convenience, the filter length in MED is set to be the same as that of VMD-AMCKD as shown in Fig. 18(b), i.e., 678. Based on this parameter setting, the MED-SK based analysis results of case 1 are shown in Fig.22.

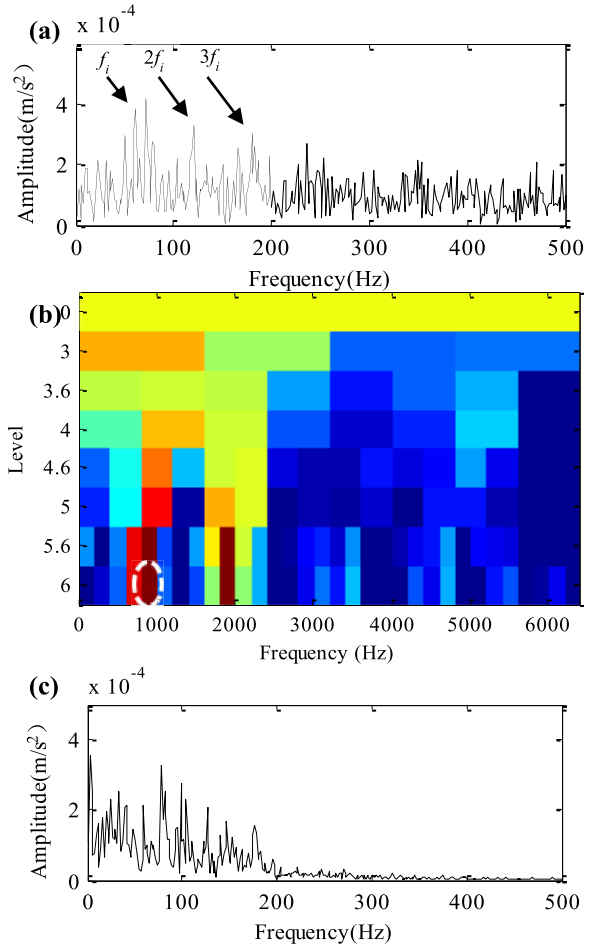

FIGURE 22. Case 1: The results obtained from MED-SK approach: (a) the envelope spectrum after MED analysis; (b) kurtogram of the signal after MED analysis; (c) envelope spectrum of the final filtered signal.

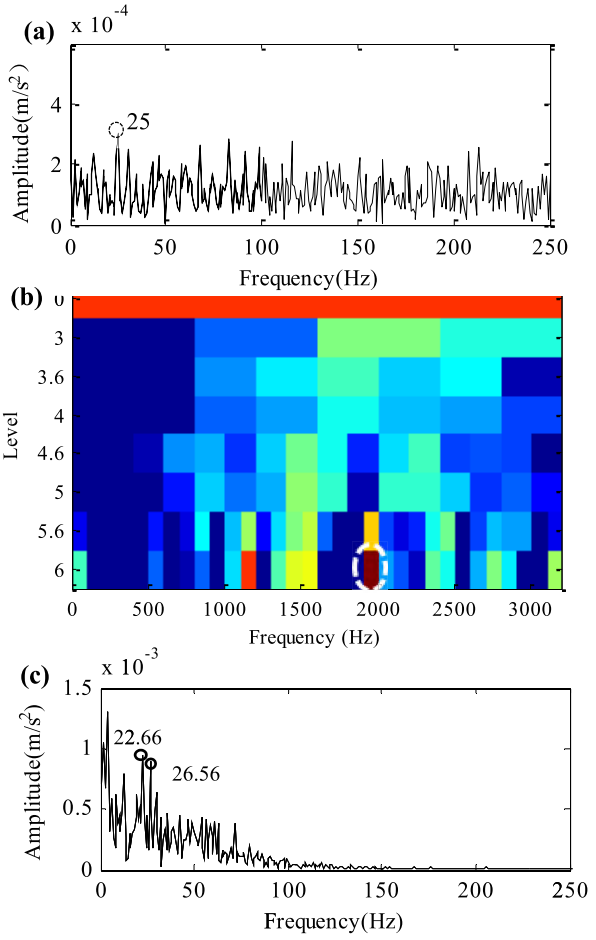

FIGURE 23. Case 2: The results obtained from MED-SK approach: (a) the envelope spectrum after MED analysis; (b) kurtogram of the signal after MED analysis; (c) the envelope spectrum of the final filtered signal.

After MED analysis, the fault frequency f_i and its multiple frequencies can be seen in Fig. 22(a). This also proves that the selection of parameter L is correct. Fig. 22(b) is the kurtogram of the filtered signal analyzed through SK method. The darkest color block (marked with the dotted ellipse) is on the sixth floor. It means the bandwidth of filtering is set to be 800-1000 Hz. In the final filtered signal envelope spectrum as illustrated in Fig. 22(c), the most protruding line is 78.13 Hz which, however, does not correspond to the fault frequency. Therefore, the MED-SK approach maybe fail in extracting the fault information from raw signals with heavy background noise.

2) MED-SK BASED DETECTING FOR ROLLING ELEMENT DAMAGE OF ROLLING BEARING

For rolling element damage of rolling bearing, the MED filter length L is set to be the same as that of VMD-AMCKD as illustrated in Fig. 21(b), i.e., 656. Fig. 23 shows the MED-SK based results of case 2.

Fig. 23(a) shows the envelope spectrum obtained from MED algorithm. From this figure, one may find that the spectra line with the largest amplitude is located at 25 Hz. As can be found from Fig. 23(b), the darkest color block (marked with dotted ellipse) in kurtogram is located at the sixth level. This means that the bandwidth of filtering is set as 1900-2000 Hz. From envelope spectrum of the final filtered signal as illustrated in Fig. 23(c) that there are two protruding frequencies of 22.66 Hz and 26.56 Hz. Unfortunately, these two frequencies are not corresponding to the fault frequency of 24.12 Hz. This implies that the MED-SK approach fails to detect incipient damage of bearing rolling element.

From the above analysis and comparison, the effectiveness of VMD-AMCKD to obtain fault characteristic information of wind turbine rolling bearing with incipient damages is verified and highlighted.

VII. CONCLUSIONS

This paper proposes VMD-AMCKD method for detecting incipient damages of rolling bearing in wind turbines. The VMD-AMCKD method can effectively suppress white Gaussian noise, non-Gaussian noise, several non-periodic impulses and can detect weak bearing faults under low SNR. The effectiveness and robustness of the VMD-AMCKD is

proved by six cases including one inner race fault model, three cases from CWRU and two cases from our laboratory wind turbine simulator. The diagnostic results of these cases obtained from VMD-AMCKD are better than those obtained from the methods proposed in [26]–[29]. The advantages and innovations of the method proposed in this paper are summarized and listed in the following.

(1) The method of center frequency observation is used to determine the mode number K in VMD, which can avoid mode aliasing.
(2) A new composite index *CEc* is constructed for selecting the most sensitive mode, which takes into account the impact information in the optimal component and considers the correlation between the component signal and the original signal.
(3) The bandwidth for solving the *CEc* indicator is limited, which can suppress the influence of random interfering frequencies.
(4) Adaptive selection of MCKD parameters is achieved by using GOA, which can avoid faulty diagnosis caused by artificial parameters.

REFERENCES

[1] B. Greening and A. Azapagic, "Environmental impacts of micro-wind turbines and their potential to contribute to UK climate change targets," *Energy*, vol. 59, pp. 454–466, Sep. 2013.
[2] X. Sun, D. Huang, and G. Wu, "The current state of offshore wind energy technology development," *Energy*, vol. 41, no. 1, pp. 298–312, May 2012.
[3] W. Y. Liu, J. G. Han, and J. L. Jiang, "A novel ball bearing fault diagnosis approach based on auto term window method," *Measurement*, vol. 46, no. 10, pp. 4032–4037, 2013.
[4] Y. Lei, Z. Qiao, X. Xu, J. Lin, and S. Niu, "An underdamped stochastic resonance method with stable-state matching for incipient fault diagnosis of rolling element bearings," *Mech. Syst. Signal Process.*, vol. 94, pp. 148–164, Sep. 2017.
[5] Z. Feng, M. Liang, Y. Zhang, and S. Hou, "Fault diagnosis for wind turbine planetary gearboxes via demodulation analysis based on ensemble empirical mode decomposition and energy separation," *Renew. Energy*, vol. 47, pp. 112–126, Nov. 2012.
[6] X. Zhang, Q. Miao, H. Zhang, and L. Wang, "A parameter-adaptive VMD method based on grasshopper optimization algorithm to analyze vibration signals from rotating machinery," *Mech. Syst. Signal Process.*, vol. 108, pp. 58–72, Aug. 2018. doi: 10.1016/j.ymssp.2017.11.029.
[7] Z. Li, Z. Feng, and F. Chu, "A load identification method based on wavelet multi-resolution analysis," *J. Sound Vib.*, vol. 333, no. 2, pp. 381–391, 2014.
[8] X. Yu, F. Dong, E. Ding, S. Wu, and C. Fan, "Rolling bearing fault diagnosis using modified LFDA and EMD with sensitive feature selection," *IEEE Access*, vol. 6, pp. 3715–3730, 2018.
[9] H. Darong, K. Lanyan, M. Bo, Z. Ling, and S. Guoxi, "A new incipient fault diagnosis method combining improved RLS and LMD algorithm for rolling bearings with strong background noise," *IEEE Access*, vol. 6, pp. 26001–26010, 2018.
[10] K. Dragomiretskiy and D. Zosso, "Variational mode decomposition," *IEEE Trans. Signal Process.*, vol. 62, no. 3, pp. 531–544, Feb. 2014.
[11] S. Mohanty, K. K. Gupta, and K. S. Raju, "Comparative study between VMD and EMD in bearing fault diagnosis," in *Proc. Int. Conf. Ind. Inf. Syst. (ICIIS)*, Dec. 2014, pp. 1–4.
[12] M. Zhang, Z. Jiang, and K. Feng, "Research on variational mode decomposition in rolling bearings fault diagnosis of the multistage centrifugal pump," *Mech. Syst. Signal Process.*, vol. 93, pp. 460–493, Sep. 2017.
[13] X. Yan, M. Jia, and L. Xiang, "Compound fault diagnosis of rotating machinery based on OVMD and a 1.5-dimension envelope spectrum," *Meas. Sci. Technol.*, vol. 27, no. 7, 2016, Art. no. 075002.
[14] Z. Li, J. Chen, Y. Zi, and J. Pan, "Independence-oriented VMD to identify fault feature for wheel set bearing fault diagnosis of high speed locomotive," *Mech. Syst. Signal Process.*, vol. 85, pp. 512–529, Feb. 2017.
[15] D. Han, X. Su, and P. Shi, "Weak fault signal detection of rotating machinery based on multistable stochastic resonance and VMD-AMD," *Shock Vibrat.*, vol. 2018, Nov. 2018, Art. no. 4252438.
[16] G. L. McDonald, Q. Zhao, and M. J. Zuo, "Maximum correlated Kurtosis deconvolution and application on gear tooth chip fault detection," *Mech. Syst. Signal Process.*, vol. 33, pp. 237–255, Nov. 2012.
[17] H. Zhao and L. Li, "Fault diagnosis method of wind turbine bearing based on maximum correlated kurtosis deconvolution and variational mode decomposition," *Acta Energiae Solaris Sinica*, vol. 39, no. 2, pp. 350–358, 2018.
[18] S. Wan, X. Zhang, and L. Dou, "Compound fault diagnosis of bearings using an improved spectral kurtosis by MCDK," *Math. Problems Eng.*, vol. 2018, no. 1, 2018, Art. no. 6513045.
[19] F. Jia, Y. Lei, H. Shan, and J. Lin, "Early fault diagnosis of bearings using an improved spectral kurtosis by maximum correlated kurtosis deconvolution," *Sensors*, vol. 15, no. 11, pp. 29363–29377, Nov. 2015.
[20] G. Tang and X. Wang, "Adaptive maximum correlated kurtosis deconvolution method and its application on incipient fault diagnosis of bearing," *Proc. Chin. Soc. Electr. Eng.*, vol. 35, no. 6, pp. 1436–1444, 2015.
[21] S. Saremi, S. Mirjalili, and A. Lewis, "Grasshopper optimisation algorithm: Theory and application," *Adv. Eng. Softw.*, vol. 105, pp. 30–47, Mar. 2017.
[22] L. Zhang, G. Xiong, and W. Huang, "New procedure and index for the parameter optimization of complex wavelet based resonance demodulation," *J. Mech. Eng.*, vol. 51, no. 3, pp. 95–103, 2015.
[23] R. B. Randall, J. Antoni, and S. Chobsaard, "The relationship between spectral correlation and envelope analysis in the diagnostics of bearing faults and other cyclostationary machine signals," *Mech. Syst. Signal Process.*, vol. 15, no. 5, pp. 945–962, 2001.
[24] J. Antoni, F. Bonnardot, A. Raad, and M. El-Badaoui, "Cyclostationary modelling of rotating machine vibration signals," *Mech. Syst. Signal Process.*, vol. 18, no. 6, pp. 1285–1314, Nov. 2004.
[25] *Case Western Reserve University Bearing Data Center Website*. Accessed: Dec. 9, 2017. [Online]. Available: http://csegroups.case.edu/bearing data center/home
[26] W. A. Smith and R. B. Randall, "Rolling element bearing diagnostics using the Case Western Reserve University data: A benchmark study," *Mech. Syst. Signal Process.*, vols. 64–65, pp. 100–131, Dec. 2015.
[27] A. Moshrefzadeh and A. Fasana, "The Autogram: An effective approach for selecting the optimal demodulation band in rolling element bearings diagnosis," *Mech. Syst. Signal Process.*, vol. 105, pp. 294–318, May 2018.
[28] D. Abboud, M. Elbadaoui, W. A. Smith, and R. B. Randall, "Advanced bearing diagnostics: A comparative study of two powerful approaches," *Mech. Syst. Signal Process.*, vol. 114, pp. 604–627, Jan. 2019.
[29] N. Sawalhi, R. B. Randall, and H. Endo, "The enhancement of fault detection and diagnosis in rolling element bearings using minimum entropy deconvolution combined with spectral kurtosis," *Mech. Syst. Signal Process.*, vol. 21, no. 6, pp. 2616–2633, Aug. 2007.

JUN ZHANG received the B.S., M.S., and Ph.D. degrees from Tianjin University, China, in 2002, 2004, and 2007, respectively.

He is currently the Deputy Director of Gear Lab, Fuzhou University, where he is also a Chair Professor with the School of Mechanical Engineering and Automation. He has published over 30 international journal papers and has served as a Reviewer of related journals for years. His research interests include dynamic analysis, vibration control, and fault diagnosis.

JIANQUN ZHANG received the B.E. degree from the East China University of Technology, China, in 2017. He is currently pursuing the M.E. degree with the School of Mechanical Engineering and Automation, Fuzhou University, China.

His research interests include mechanical fault diagnosis and signal processing.

MIN ZHONG received the B.E. degree from the Henan University of Science and Technology, China, in 2017. He is currently pursuing the M.E. degree with the School of Mechanical Engineering and Automation, Fuzhou University, China.

His research interests include mechanical fault diagnosis and signal processing.

JIANHUA ZHONG received the M.S. and Ph.D. degrees in electromechanical engineering from the University of Macau, in 2011 and 2016, respectively.

He is currently an Assistant Professor with the School of Mechanical Engineering and Automation, Fuzhou University, China. He has published over 20 papers in refereed journals and conference proceedings. His research interests include rotating machinery condition monitoring, vehicle dynamics and control, signal processing, pattern recognition, and fault diagnosis using machine learning methods.

JINDE ZHENG received the B.S. degree in mathematics from the Anhui Normal University, Wuhu, China, in 2009, and the Ph.D. degree in mechanical engineering from Hunan University, Changsha, China, in 2014.

From 2014 to 2016, he was a Lecturer with the Mechanical Engineering Department, Anhui University of Technology, where he has been an Associate Professor, since 2017. He is the author of over 50 articles. His research interests include machinery health monitoring and fault diagnosis.

LIGANG YAO received the B.S. and M.S. degrees from Northeast Petroleum University, China, in 1984 and 1987, respectively, and the Ph.D. degree from the Harbin Institute of Technology, China, in 1996.

He is currently a Professor with the School of Mechanical Engineering and Automation of Fuzhou University, China. His research focuses on the design and manufacturing of innovative gear transmissions, rehabilitation robotics, and geometric modelling.